8-1-1995

Relationship between correlation function fit parameters and source distributions

Douglas E. Fields

J. P. Sullivan

J. Simon-Gillo

H. Van Hecke

B. V. Jacak

See next page for additional authors

Recommended Citation

Fields, Douglas E.; J. P. Sullivan; J. Simon-Gillo; H. Van Hecke; B. V. Jacak; and N. Xu. "Relationship between correlation function fit parameters and source distributions." *Physical Review C* 52, 2 (1995): 986-994. doi:10.1103/PhysRevC.52.986.

Relationship between correlation function fit parameters and source distributions

D. E. Fields, J. P. Sullivan, J. Simon-Gillo, H. van Hecke, B. V. Jacak, and N. Xu
Los Alamos National Laboratory, Los Alamos, New Mexico, 87545
(Received 21 March 1995)

We review the method of two-particle intensity interferometry, define appropriate techniques to make the comparison between RQMD source distributions and correlation function fit parameters, and compare these to results from CERN experiments NA44 and NA35. The fit parameters are investigated as a function of rapidity and transverse momentum and are found to depend on the collision dynamics. Although position-momentum correlations invalidate the naive interpretation of the correlation function fit parameters as source sizes, we use a dynamical model to extract this information and identify a region in rapidity and transverse momentum where the dynamical effects are minimized.

PACS number(s): 25.75.+r, 02.70.Ns

I. INTRODUCTION

From medium-energy heavy-ion facilities such as the MSU-NSCL to the highest energy accelerators such as the CERN SPS, two-particle correlation measurements have become a major part of the experimental agenda. These experiments are all driven by the desire to understand the dynamical evolution of the collision process. Since intensity interferometry was first used in nuclear physics [1], there has been much excitement about this method of determining the space-time characteristics of the interaction zone in nuclear collisions. Furthermore, the source volume and lifetime may be sensitive to the formation of a quark-gluon plasma would lead to a longer lifetime and a larger source size than hadronic matter [2]. Ideally, both quantities should be measurable through intensity interferometry.

In this work, pion correlation functions over a broad range of rapidity and transverse momentum, p_T, are derived from events generated by the RQMD model and fit with the static Gaussian formalism. The resulting fit parameters are compared to the input source distributions and to experimental results. If the formalism correctly describes the physical processes involved, the fit parameters relate directly to the source distributions. As this may not be the case, the assumptions underlying the formalism are discussed. By relating the fit parameters to the input source distributions in the simulations, more quantitative interpretations of the experimental fit parameters can be made. Although the RQMD model is used as the basis for the comparison, emphasis will be given here to effects which should not depend critically on the model, such as transverse expansion and resonance decay.

We compare our work to CERN experiments NA35 and NA44 at $E/A = 200$ GeV, S+Au and S+Pb. The radius parameters extracted in these experiments vary in a consistent manner from system to system, e.g., the radius parameters for the p+Pb system are smaller than for the S+Pb system [4]. The radius parameters are also much larger than the projectile RMS radii [5,6]. However, a more quantitative interpretation of these parameters is difficult. Lorentz effects are significant and are highly dependent on the collision dynamics. The dynamics of the particle emission can also be complex. Thus, parameters derived from fitting experimental data to a static, spherically symmetric, Gaussian model are not easy to interpret. Most of the conclusions drawn from the behavior of the radius parameters have been qualitative. More quantitative information about the source size, amount of transverse and longitudinal expansions, and the shape of the freeze-out distribution can be extracted from detailed simulations of the collisions [6–8].

Section II of this paper reviews the standard method of intensity interferometry, as well as the RQMD model and experimental data. In Sec. III a relatively uncomplicated method for making direct comparisons between simulated correlation functions and source properties is given, with the results of this study presented in Sec. IV. In Sec. V results of this comparison are discussed in light of the experimental results from CERN experiments NA35 and NA44. A discussion of these comparisons and the global trends of the RQMD model is given in Sec. VI. Conclusions are drawn in Sec. VII.

II. REVIEW

We briefly review the intricacies of intensity interferometry in nuclear physics, although more complete descriptions exist elsewhere [9,10]. Throughout this review, we emphasize the assumptions usually made in the analysis of two-particle correlation data. We will later analyze the effect of deviations from these assumptions on the interpretation of the results.

The amplitude of detection of two identical bosons from a source with emission (space-time) points and momenta $\mathbf{x}_1, \mathbf{p}_1$ and $\mathbf{x}_2, \mathbf{p}_2$ is written as

$$A_{12} = \frac{1}{\sqrt{2}}[e^{i\mathbf{p}_1\cdot(\mathbf{r}_1-\mathbf{x}_1)}e^{i\mathbf{p}_2\cdot(\mathbf{r}_2-\mathbf{x}_2)} + e^{i\mathbf{p}_1\cdot(\mathbf{r}_1-\mathbf{x}_2)}e^{i\mathbf{p}_2\cdot(\mathbf{r}_2-\mathbf{x}_1)}] , \quad (1)$$

where $\mathbf{r}_1, \mathbf{r}_2$ are the points of detection for particles of momenta $\mathbf{p}_1, \mathbf{p}_2$, respectively. It is assumed that the boson wave functions can be described as plane waves, i.e., the particles undergo no strong interactions.

The probability of detecting such a pair is given by the amplitude squared integrated over the source distribution

$$P_{12} = \int d^4\mathbf{x}_1 d^4\mathbf{x}_2 |A_{12}|^2 \rho(\mathbf{x}_1)\rho(\mathbf{x}_2) \ , \tag{2}$$

where $\rho(\mathbf{x})$ is the space-time distribution of bosons in the source. If the space-time distributions are independent of momentum, and if they are mutually independent of each other (incoherent), then the integral separates and reduces to

$$P_{12} = 1 + |\rho(\mathbf{q})|^2 \equiv C_2^{\text{ideal}}(\mathbf{q}) \ , \tag{3}$$

where $\mathbf{q}$ is the four-momentum $(q_0, \vec{p}_2 - \vec{p}_1)$ and C_2^{ideal} is what we will refer to as the correlation function. This is the "traditional" interpretation of the correlation function, i.e., that it is one plus the Fourier transform of the position distribution. Deviations from the assumptions would lead to a modification of this interpretation.

It has been shown that the correlation function is not a true four-dimensional function of $\mathbf{q}$ [9]; that is, since $q_0 = \vec{q} \cdot \vec{\beta}_{12}$, with

$$\vec{\beta}_{12} \equiv \frac{\vec{p}_1 + \vec{p}_2}{|E_1 + E_2|} \ , \tag{4}$$

the width of the emission time distribution is measured along with the component of $\vec{q}$ parallel to the pair momentum. Consequently, a wise choice of the coordinates for three-dimensional analysis of an experimental correlation function would include one component of the momentum difference in the direction of the pair momentum (Q_{T_0}). A second natural choice would put one component (Q_L) in the direction of the beam (z in this paper), since one would expect symmetry around this axis. This leaves the third component defined as orthogonal to these (Q_{T_s}) [2,11].

With this coordinate system, the assumptions defined above and the additional assumption of a spherically symmetric Gaussian source distribution given by

$$\rho(\mathbf{x}) \propto e^{-|\vec{x}|^2/2R^2 - |t|^2/2\tau^2} \ , \tag{5}$$

where R and τ are the widths of the spatial and temporal distributions, respectively, the correlation function becomes

$$C(Q_{T_0}, Q_{T_s}, Q_L)$$

$$= A[1 + \lambda \exp(-Q_{T_0}^2 R_{T_0}^2 - Q_{T_s}^2 R_{T_s}^2 - Q_L^2 R_L^2)] \ , \tag{6}$$

where the phenomenological parameter λ is the chaoticity or strength parameter and has the value of one in the ideal case [12]. By examining the relationship of this correlation function to its inverse Fourier transform and to Eqs. (1) and (2), the radius parameters relate to R (the width of the position distribution) by [10]

$$R_L^{\text{exp}} = \sqrt{\gamma_s^2[R^2 + U_s^2\tau^2]} \ , \tag{7}$$

$$R_{T_s}^{\text{exp}} = R \ , \tag{8}$$

$$R_{T_0}^{\text{exp}} = \sqrt{\gamma_s^2[(1 - U_s^2\beta_{12}^2)R^2 + \beta_{12}^2\tau^2]} \ , \tag{9}$$

where $\gamma_s \equiv 1/\sqrt{1 - U_s^2}$, U_s is the source velocity in the analysis frame, and τ is the width of the source lifetime distribution. In this work, we will use the $P_z = p_{z1} + p_{z2} = 0$ frame [the longitudinal center-of-mass frame (LCMS)], such that $U_s = 0$ and $\gamma_s = 1$ for Lorentz invariant longitudinal expansion. The assumption of Lorentz invariant longitudinal expansion has been shown to be valid experimentally by the NA35 analysis in the nucleon-nucleon center-of-mass frame [5]. Thus, the assumption of spherical symmetry can be relaxed to a cylindrical symmetry [13]. The radius parameters then relate to R_L and R_T, the longitudinal and transverse widths of the position distribution, by

$$R_L^{\text{exp}} = \sqrt{\gamma_s^2[R_L^2 + U_s^2\tau^2]} \ , \tag{10}$$

$$R_{T_s}^{\text{exp}} = R_T \ , \tag{11}$$

$$R_{T_0}^{\text{exp}} = \sqrt{\gamma_s^2[(1 - U_s^2\beta_{12}^2)R_T^2 + \beta_{12}^2\tau^2]} \ . \tag{12}$$

Experimentally, the probability for detecting a correlated pair (the correlation function) is determined by

$$C_2^{\text{exp}}(\vec{q}) = \frac{A(\vec{q})}{B(\vec{q})} \ . \tag{13}$$

The "real distribution" $A(\vec{q})$ is the measured two-particle distribution as a function of the relative momentum, and the "background distribution" $B(\vec{q})$ is typically a two-particle distribution constructed from tracks mixed randomly from all events contained in $A(\vec{q})$.

Several corrections must be applied to Eq.(13) before Eq. (6) may be used to extract dynamical quantities from the correlation function. The background distribution $B(\vec{q})$ ideally should consist of completely uncorrelated pairs. Experimentally, however, if the sample of pairs from which the background distribution is created contains correlations (e.g., from the Bose-Einstein correlation), a residual correlation will remain in the mixed-pair events [10]. Additionally, effects of the detector acceptance must be eliminated from the pair sample. Finally, because of the assumption of noninteracting particles (plane waves), any final state and Coulomb interactions must be taken into consideration.

Both NA35 and NA44 have large two-pion data samples for sulphur on heavy target reactions at $E/A = 200$ GeV, allowing three-dimensional analysis of the correlation function. NA44 has particle identification capability to separate pions and kaons. NA35 has a broad acceptance and one can study rapidity as well as p_T dependences of the correlation functions. The data analysis

methods are similar but the functions used in fitting the data differ slightly. Both experiments assume a Gaussian position distribution, leading to a Gaussian-like correlation function. NA35 has an additional factor of $\frac{1}{2}$ in the exponent of Eq. (6), resulting in quoted fit parameters that are larger by a factor of $\sqrt{2}$. Also, the NA44 analysis is in the LCMS frame, whereas NA35 uses the N-N center-of-mass frame. Comparison of the resulting fit parameters requires conversion to a common reference frame.

Experiments have compared their data to the RQMD model with good agreement [4,6–8,14,15]. The RQMD model (version 1.08) is a transport-type event generator based on string and resonance excitation and decay and includes rescattering of the produced particles. It also includes string-string interactions (color ropes). A detailed description can be found elsewhere [16]. Two-particle correlation functions are calculated via the method described in Ref. [15].

The simulated correlation function is determined by

$$C_2^{\rm calc}(\vec{q}) = \sum_{i=1}^{N(q)} \frac{A_{12_i}(\vec{q})}{N(\vec{q})} , \qquad (14)$$

where $N(\vec{q})$ is the number of pairs in each $\vec{q}$ bin. The numerator is analogous to the number of pairs measured in an experiment and the denominator, $N(\vec{q})$ is analogous to the number of pairs in the background sample. A_{12} uses the Coulomb plus strong interaction wave function for charged pions, so, as for experimental data, the correlation function is corrected for the Coulomb interaction using the Gamow factor [12]. Since the Gamow factor assumes a point source, a small error is introduced in the Coulomb correction to the correlation function.

III. METHOD

The relatively good agreement between calculated correlation functions from RQMD and experimental results, in addition to good agreement with measured single-particle spectra [17,18] indicate that RQMD can be used as a tool to study the position, momentum, and time distributions of particles at freeze-out. A global study of the relationship between the fit parameters and the source distributions may identify areas of particular sensitivity (or insensitivity) to collision dynamics. Also, systematic differences in the fit parameters from different experiments may be understood in this way.

In this study, events from the RQMD simulation of 200 GeV/A, S+Pb collisions were separated into 38 bins in rapidity and transverse momentum of the pair calculated in the LCMS frame. Bin sizes were chosen to have sufficient statistics in each bin, given the size of the simulated event sample. At mid-rapidity and low transverse momentum, bins were one-half unit of rapidity and 100 MeV/c in transverse momentum. At the extremes of rapidity, the bins were one unit of rapidity and 200 MeV/c in transverse momentum. Bins of 200 MeV/c in transverse momentum were also used at high p_T at mid-rapidity. No azimuthal angle restriction was used in the acceptance for each bin, i.e., only rapidity and transverse momentum were used to select events for that bin. Particles were taken from "minimum bias" events from a range of impact parameters (0–7 fm).

For each bin, a correlation function was calculated as in Ref. [15] with 15 MeV/c bin sizes in momentum difference projections. These correlation functions were then used to fix the parameters of Eq. (6) via a simultaneous fit to the three dimensions with a single value of λ. Although this method is not a full three-dimensional fit to the correlation function, the effect of projecting the full three-dimensional function onto the axis is taken into account in the fitting procedure. Examples of the correlation functions and fits are shown in Figs. 1(a) and 1(b) for two different p_T bins.

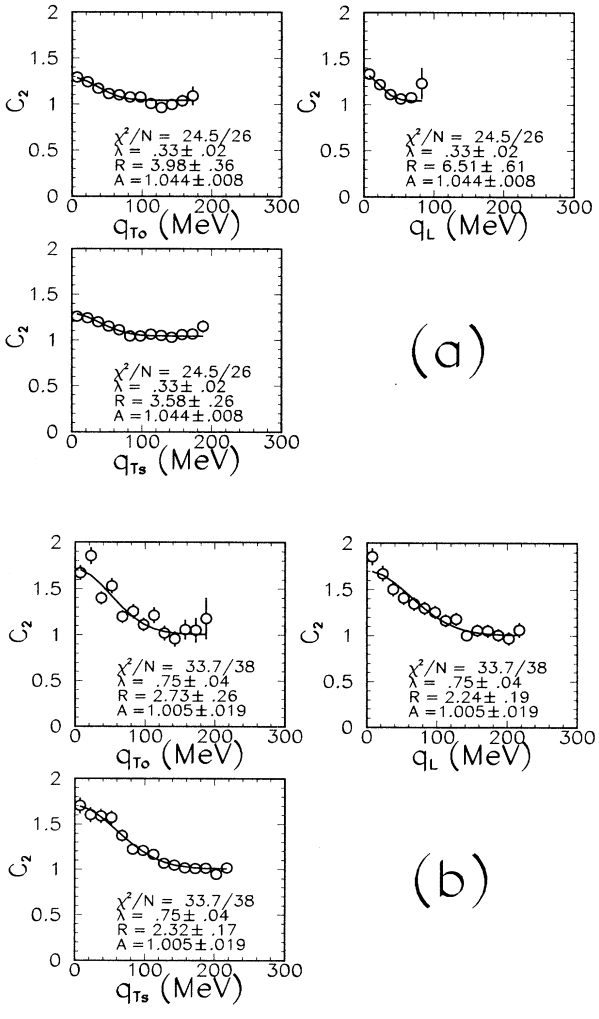

FIG. 1. Two-pion correlation functions and fits from E/A = 200 GeV, S+Pb RQMD events for rapidity between 2.75 and 3.25 and for (a) P_T between 0 and 100 MeV/c and (b) P_T between 600 and 800 MeV/c events.

In addition to the fit parameters, the freeze-out distribution of particles was examined for each bin in rapidity and p_T. As previously mentioned, the relationship between the source distributions and the fit parameters from the simulations is straightforward when the assumptions of the formalism are valid. Lorentz effects, correlation between the position and momentum, resonance decays, and time-dependent dynamics can alter this relationship. It is shown in the next section that the effects are indeed significant, and that they necessitate the use of a model to determine source properties from experimental data.

IV. RESULTS

Figure 2 shows the fit parameters λ, R_{T_0}, R_L, and R_{T_s} as a function of rapidity versus transverse momentum, p_T, from correlation functions calculated from RQMD events. The acceptance of each bin is given in Table I as well as the value and error of the fit parameters from that bin. The general trends of the fit parameters are as follows. (1) The λ parameter is independent of rapidity and is a strong functions of transverse momentum, rising from near 0.3 at $p_T = 0$ and approaching 0.8 at $p_T = 800$ MeV/c. This is shown below to be caused by the relative fraction of particles originating from long distances ($R > 20$ fm/c) and is mainly due to resonance decay. (2) The radius parameters exhibit a more complex shape, peaking at mid-rapidity and low transverse momentum. R_L demonstrates the strongest p_T dependence, falling from nearly 7 fm at low p_T to 2 fm at $p_T = 800$ MeV/c. The behavior of R_{T_s} is similar to that of R_{T_0}.

The difference between the two transverse radius parameters should ideally measure the emission time difference between the particles of the pair. From Eqs. (11) and (12) in the $P_z = 0$ reference frame,

$$\Delta\tau = \sqrt{(R_{T_0}^2 - R_{T_s}^2)}/\beta_{\pi\pi} \ . \tag{15}$$

TABLE I. Fit parameters for $\pi\pi$ correlation functions created from $E/A = 200$ GeV, S+Pb RQMD events. Equation (6) is used is the fitting function.

p_T	y	0.75–1.75	1.75–2.25	2.25–2.75	2.75–3.25	3.25–3.75	3.75–4.25	4.25–5.25
0–0.1	λ		0.33±0.02	0.37±0.02	0.33±0.02	0.30±0.02	0.34±0.03	
	R_{T_0}		3.98±0.34	4.29±0.31	3.98±0.36	3.74±0.43	3.73±0.43	
	R_{T_s}		3.76±0.29	3.61±0.27	3.58±0.26	2.96±0.28	2.94±0.34	
	R_L		5.83±0.64	6.78±0.55	6.51±0.61	5.95±0.83	6.68±1.02	
0–0.2	λ	0.33±0.02						0.38±0.02
	R_{T_0}	3.02±0.29						2.83±0.20
	R_{T_s}	2.84±0.20						2.66±0.21
	R_L	4.90±0.60						4.16±0.35
0.1–0.2	λ		0.40±0.02	0.41±0.02	0.41±0.02	0.47±0.02	0.43±0.02	
	R_{T_0}		4.25±0.32	3.91±0.34	4.07±0.30	4.34±0.37	3.57±0.35	
	R_{T_s}		3.03±0.22	2.99±0.23	3.39±0.25	2.87±0.17	2.88±0.17	
	R_L		4.13±0.34	5.09±0.43	3.86±0.36	4.49±0.35	4.84±0.50	
0.2–0.3	λ		0.48±0.02	0.43±0.02	0.51±0.02	0.48±0.02	0.50±0.03	
	R_{T_0}		3.92±0.31	3.40±0.34	3.21±0.29	3.76±0.35	3.38±0.30	
	R_{T_s}		2.77±0.18	2.60±0.21	2.80±0.16	2.88±0.20	2.56±0.18	
	R_L		3.87±0.32	3.79±0.32	3.72±0.27	3.58±0.30	3.53±0.30	
0.2–0.4	λ	0.46±0.03						0.53±0.03
	R_{T_0}	2.78±0.29						3.08±0.28
	R_{T_s}	2.46±0.23						2.57±0.17
	R_L	2.90±0.29						3.47±0.35
0.3—0.4	λ		0.58±0.03	0.55±0.02	0.59±0.03	0.57±0.03	0.60±0.12	
	R_{T_0}		3.58±0.30	3.72±0.30	3.50±0.27	3.91±0.29	3.19±1.27	
	R_{T_s}		2.93±0.17	2.52±0.14	3.00±0.16	2.67±0.15	2.45±0.65	
	R_L		3.76±0.28	3.07±0.23	2.94±0.18	2.80±0.20	3.07±0.92	
0.4–0.6	λ	0.66±0.04	0.62±0.03	0.57±0.03	0.61±0.03	0.60±0.03	0.70±0.03	0.64±0.04
	R_{T_0}	2.83±0.25	2.82±0.24	3.34±0.27	2.97±0.21	3.22±0.26	2.93±0.22	2.90±0.29
	R_{T_s}	2.23±0.16	2.64±0.17	2.68±0.22	2.35±0.17	2.52±0.16	2.33±0.14	2.28±0.17
	R_L	2.54±0.20	2.46±0.18	2.78±0.21	2.15±0.16	2.49±0.18	2.44±0.19	2.03±0.19
0.6–0.8	λ	0.80±0.05	0.67±0.04	0.74±0.04	0.75±0.04	0.74±0.05	0.79±0.08	0.73±0.10
	R_{T_0}	3.15±0.31	2.61±0.29	2.58±0.21	2.73±0.26	2.29±0.25	2.21±0.31	2.39±0.49
	R_{T_s}	2.62±0.22	2.61±0.23	2.48±0.19	2.32±0.17	2.32±0.20	2.02±0.23	2.07±0.37
	R_L	2.40±0.22	2.33±0.22	2.15±0.16	2.24±0.19	1.96±0.17	1.67±0.23	1.63±0.32

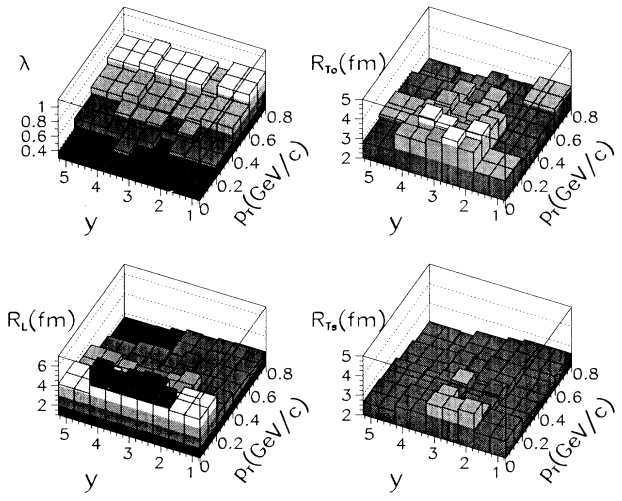

FIG. 2. Fit parameters from pion correlation functions derived from $E/A = 220$ GeV, S+Pb RQMD events as a function of rapidity y, and transverse momentum p_T. Acceptances in rapidity and p_T for the correlation functions are as listed in Table I. (Note that at low and high rapidity and at high p_T the acceptance are more than one bin.)

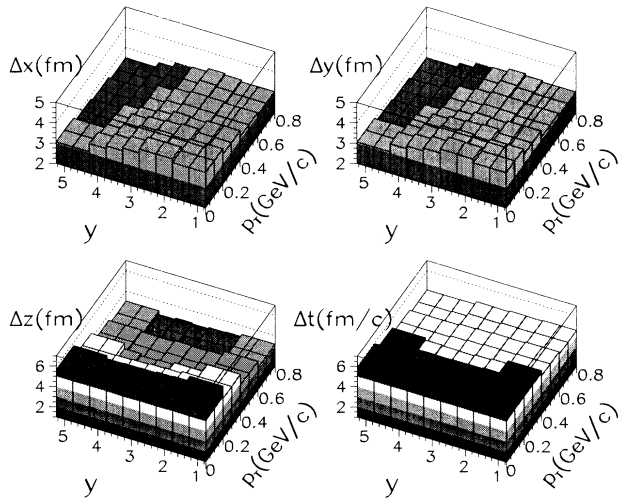

FIG. 4. The widths of the space-time distributions for the same events used to calculate the correlation functions of Fig. 2 (see text for details).

Figure 3 shows this $\Delta\tau$ in the rapidity versus p_T plane. The values decrease from 6 fm/c at mid-rapidity and low p_T to 1 fm/c at high p_T.

For comparison to the fit parameters, the source space-time distributions at freeze-out from RQMD are plotted for each bin in rapidity and p_T in the LCMS frame. Figure 4 shows $1/\sqrt{2}$ RMS width of the distance between particles at freeze-out. (The factor of $1/\sqrt{2}$ is needed for comparison to the fit parameters, since the difference of two Gaussian distributions of equal width is wider than the original distributions by this factor). The difference distributions were used instead of the positions so that they would always be centered on zero. This allows a fixed range for the RMS of ±20 fm. Shown in Fig. 4 are the resulting x, y, z (beam direction) and time t widths as a function of rapidity and p_T.

The x and y distributions are the same because events were rotated round the beam axis to increase statistics for pairs in the rapidity and p_T acceptance. The values decrease from approximately 4 fm at low p_T to near 3

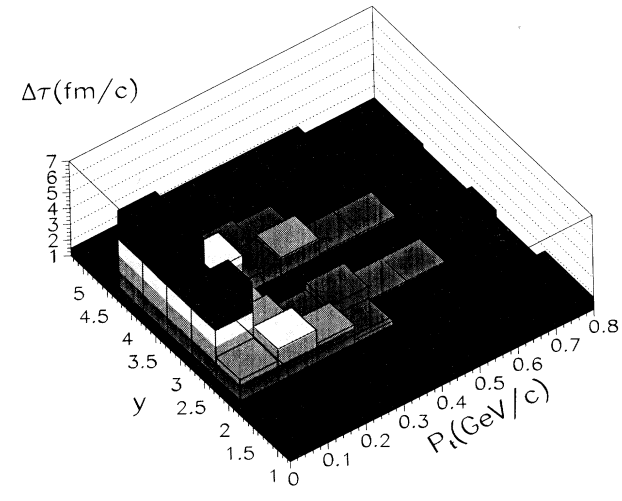

FIG. 3. The width of the emission time distribution τ as calculated from R_{T_0} and R_{T_s} from Table I and Eq. (15). The value of the pair velocity, $\beta_{\pi\pi}$, is determined from the mean p_T in the acceptance.

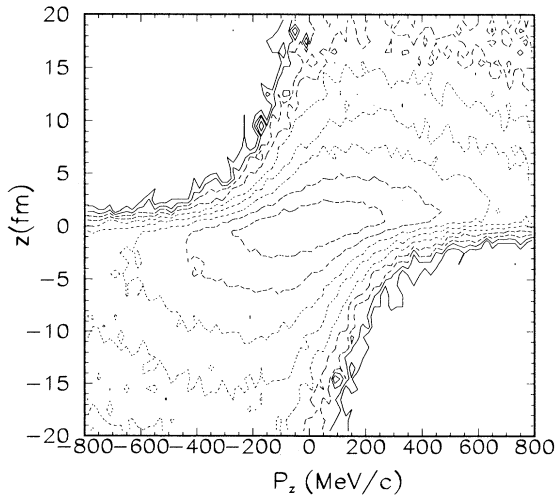

FIG. 5. Plot of p_y versus y position for all pions from RQMD simulation of $E/A = 200$ GeV, S+Pb collisions. A correlation between freeze-out position and momentum can be clearly seen.

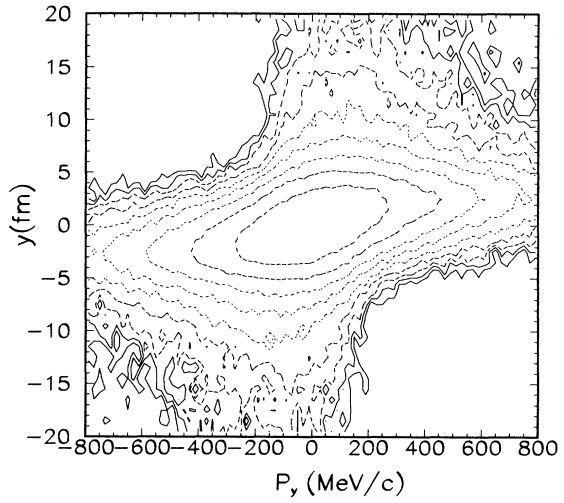

FIG. 6. Plot of p_z versus z position for all pions from RQMD simulation of $E/A = 200$ GeV, S+Pb collisions. The correlation between freeze-out position and momentum in the longitudinal direction is seen to be stronger than that for the transverse direction, Fig. 5.

fm at $p_T = 0.8$ GeV/c. There is also a slight rapidity dependence. The p_T dependence of the z distribution is much more striking, falling from 6 fm at low p_T to 3 fm at $p_T = 0.8$ GeV/c. The z distribution shows little rapidity dependence. A slight p_T dependence can be seen in the width of the freeze-out time distributions, decreasing from 6 fm/c at low p_T to 4.5 fm/c at $p_T = 0.8$ GeV. There is no rapidity dependence of the emission lifetime.

In order to examine the distribution of particles with similar momenta, an additional requirement that p_x be greater than zero was imposed. This requirement is unnecessary if the position and momenta of the particles are uncorrelated, as assumed in the derivation of the fitting function. However, as shown in Figs. 5 and 6, pions at freeze-out in the RQMD simulation are correlated in position and momentum. Particles with positive p_y are more likely to be found at positive y. The effect of this correlation can be seen in the widths of the y position distribution as a slight decrease with increasing p_T, reminiscent of the same trend in the R_{T_s} fit parameter of Fig. 2.

V. COMPARISON TO DATA

Although comparisons of data to RQMD are naturally made by applying the detector acceptance to the RQMD events, it is informative to compare the experimental results to the global RQMD trends. One would not expect quantitative agreement since experimental acceptances are, in general, more complicated than rectangular bins in rapidity and p_T. It is also important to have the same collision dynamics bias in the simulations as the experimental data. Furthermore, both the experimental and simulated fit parameters must be determined in the same rest frame and using the same fitting function.

Table II is a compilation of the available data from the NA35 and NA44 experiments compared to the results from comparable rapidity and p_T of the calculation. Also included in the table is the RQMD result using the NA44 detector acceptance for the low and high p_T data sets. The agreement is generally good for both experiments. The differences between the experiments can be qualitatively understood as arising from the differing rapidity and p_T coverage.

TABLE II. Comparison of fit parameters from NA35 and NA44 $\pi\pi$ correlations to those of Table I. NA44 data is for $E/A = 200$ GeV, S+Pb, NA35 data is for $E/A = 200$ GeV, S+Au. NA35 data has been converted to the LCMS frame and reduced by the factor of $\sqrt{2}$ to conform with the present formalism. "This work" is the RQMD results of Table I using square acceptances in rapidity and p_T. "RQMD+NA44" is a RQMD calculation using the NA44 experimental acceptance and bias.

$\langle y \rangle$	$\langle p_T \rangle$	Ref.	λ	R_{T_0}	R_{T_s}	R_L
2.7	0.45	[6]	0.59±0.02	3.0 ± 0.2	3.0 ± 0.2	3.1 ± 0.2
		This work	0.61±0.03	3.16±0.27	2.52±0.22	2.46±0.21
		RQMD+NA44	0.76±0.27	4.21±0.24	3.23±0.27	3.37±0.15
3.5	0.15	[6]	0.56±0.02	4.0 ± 0.1	4.2 ± 0.3	4.7 ± 0.3
		This work	0.41±0.02	4.34±0.37	2.87±0.17	4.49±0.35
		RQMD+NA44	0.71±0.03	4.25±0.23	4.55±0.27	6.52±0.48
4.0	0.10	[5]		3.5 ± 0.3	3.1 ± 0.3	6.2 ± 0.4
4.0	0.10	This work[a]	0.38±0.03	3.65±0.39	2.91±0.26	5.76±0.76
4.0	0.20	[5]		3.4 ± 0.2	3.2 ± 0.2	5.0 ± 0.3
4.0	0.20	This work[a]	0.46±0.03	3.47±0.32	2.72±0.18	4.18±0.40
4.0	0.30	[5]		2.9 ± 0.3	3.1 ± 0.3	5.1 ± 0.4
4.0	0.30	This work[a]	0.55±0.08	3.28±0.78	2.50±0.42	3.30±0.61
4.0	0.45	[5]		2.5 ± 0.4	2.8 ± 0.4	4.0 ± 0.5
4.0	0.45	This work[a]	0.65±0.08	3.06±0.74	2.39±0.40	2.76±0.56

[a]Two p_T bins are averaged.

VI. DISCUSSION

This global study allows the following: (1) A global picture of the trends of the fit parameters, with the ability to manipulate the input to the event sample and thus gain a better understanding of the underlying physics; (2) understanding the meaning of the fit parameters by comparison between the fit parameters and the source distributions; (3) comparison of results from experiments to the model and interpret the results in terms of the source distributions in the model; (4) comparison of results from different experiments. We will discuss each of these in turn.

How does one interpret the trends in the fit parameters? It has been shown [15,19,20] that the presence of long-lived resonance, predominant at low p_T, can suppress the expected value of the λ parameter by creating a very narrow component in the correlation function. When the **q** resolution of the detector (real or simulated) is larger than this narrow component, the spike gets smeared into several bins of **q** and the correlation function does not go to 2 as expected. The resulting λ is less than the ideal value of 1. This is not an effect of a coherent source as the name "chaoticity parameter" implies. It has also been speculated that the presence of long-lived resonances may lead to observed the p_T dependence of the radius parameters [6]. Resonance decays populate low p_T because of momentum sharing between multiple decay products.

In order to better understand the effect of resonance decay on the fit parameters, we repeated the above process with all pions originating from long-lived resonances (ω, η, η') excluded from the sample comprising the correlation function. Figure 7 shows the relative fraction of each of these resonances as well as the total fraction of long-lived resonances as a function of rapidity and transverse momentum. The long-lived resonance fraction starts near 30% at low p_T and falls to 5% at $p_T = 0.8$ GeV/c. (The apparent rapidity dependence at low p_T is from the larger range of p_T at low and high rapidity.)

Figure 8 shows the fit parameters from correlation functions derived from the same events as above, but excluding the long-lived resonance decay products. In order to avoid errors in approximating the effect of Coulomb forces, the Coulomb part of the wave function was turned off in the calculation and the Gamow correction was not applied. The most notable change from Fig. 2 is in the λ parameter, where the value is now approximately 1 except at mid-rapidity and very low p_T. Even with these resonances removed, at mid-rapidity and $p_T < 100$, 20% of the pions have a freeze-out radius greater than 40 fm. This accounts for the remaining depression of the correlation function intercept in this region.

Resonances do not appear to be the cause of the p_T dependence of the radius parameters as very little change in the trends of the radius parameters is seen when the resonance decay products are excluded. The only significant change is in R_{T_0} where the overall value increases somewhat. This is a rather surprising result, since we are excluding most of the large radius component. However, examination of the width from a Gaussian fit to the position distribution (rather than the RMS) for events excluding these long-lived resonances show very little difference from the full event sample.

We can refer back to Eqs. (10)–(12) to relate the RQMD fit parameters to the widths of the source distributions. From Eq. (11), R_{T_s} is related directly to the width of the position distribution. Comparing R_{T_s} from Fig. 2 to the y widths of Fig. 4, one sees that the values of R_{T_s} are consistently 20% smaller than the position widths. R_{T_0} from Eq. (12) should be a combination of both the position width and the emission time width times the pair velocity. From the position and time dis-

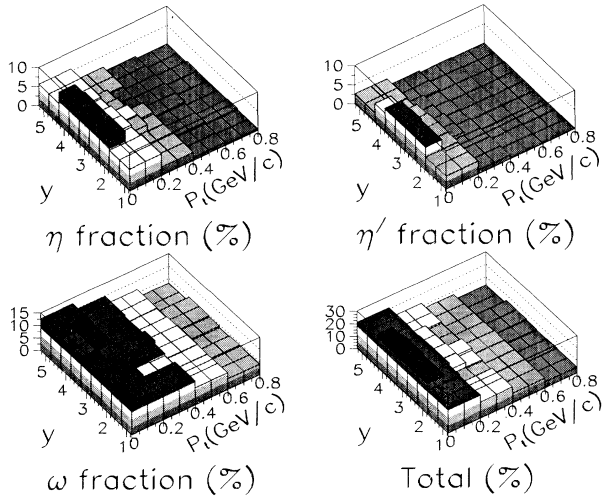

FIG. 7. Relative fraction of pions from resonance decay for three of the most important long-lived resonances. The total fraction of pions from these resonances is also shown.

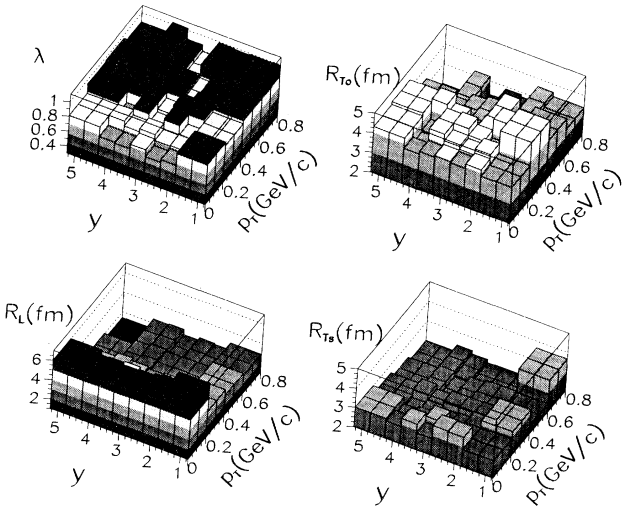

FIG. 8. Fit parameters from correlation functions derived from the same events as Fig. 2, with the resonances of Fig. 7 excluded. The Coulomb part of the wave function was also omitted and no Gamow correction applied.

tributions, R_{T_0} should have a value of around 8 fm. Yet, as seen from Fig. 2, R_{T_0} has a maximum value of around 4.5 fm at $p_T = 0.3$ GeV/c and then falls to smaller values at high p_T.

Although R_{T_0} is somewhat larger when the resonances are excluded (Fig. 8), it is still much smaller than the 8 fm expected in the ideal case [see Eq. (12) and Fig. 4]. This effect can be clearly demonstrated by comparing the distribution of Fig. 9 with the time distribution of Fig. 4. At low p_T and mid-rapidity, Eq. (15) gives a good description of the emission lifetime, whereas at high p_T, it falls 5–6 fm/c short of the emission lifetime.

The p_T dependence of the radius parameters in the experimental data is shown by the model to be a result of the correlation between position and momentum within the source at freeze-out. This correlation between position and momentum may be caused by transverse expansion driven by rescattering of the particles [21]. Because of this expansion, a smaller fraction of the total source size is probed at higher p_T. Without a model, one cannot quantitatively determine the effects of the transverse and longitudinal expansion on the different radius parameters. Qualitatively, however, since R_{T_0} is oriented in the direction of the transverse expansion, it is affected to a greater degree than R_{T_s}, which probes the dimension perpendicular to the transverse expansion. This leads to a smaller value of τ derived from these two parameters at high p_T.

Table II demonstrates the difficulties in making direct comparisons between different experimental results. There is one set of NA35 and NA44 measurements of similar average rapidity and p_T with somewhat different results. However, by comparing the RQMD results of this work to that with the NA44 acceptance, it is clear that the details of the shape of the acceptance as well as any event sample biases are important. Since both experimental results are reproduced by the RQMD simulations, one can say that the NA35 and NA44 results are consistent.

As stated previously, the comparison of the experimental results to RQMD is best done by applying the experimental acceptance and event sample bias to the stimulated events, and then constructing the correlation functions. However, the current study allows us to compare the simulated fit parameters to the source distributions at all rapidity and p_T, and identify areas in rapidity and p_T space where the fit parameters most closely represent the "true" source distributions. The lifetime and transverse size of the source are shown to be best measured at mid-rapidity and low p_T.

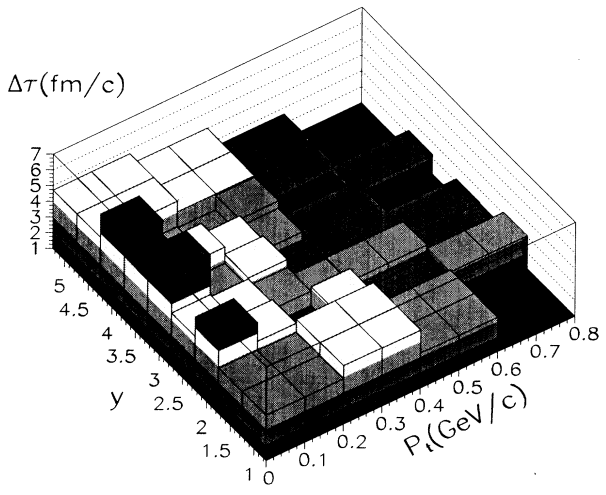

FIG. 9. The width of the emission time distribution τ as calculated from R and R_{T_s} from Fig. 8 and Eq. (15).

VII. CONCLUSIONS

The results from experimental two-particle correlation functions are difficult to interpret without the aid of microscopic models. The assumptions which enter into the derivation of fitting functions for the experimental correlations are not all valid according to the RQMD model. These difficulties can be overcome by comparing the results of a global study of correlation functions derived from RQMD events, the source space-time distributions of these events, and the experimental results. Another approach may be to use a formulation which takes into account the dynamics of the collision, and therefore yields fit parameters which can be interpreted more directly [22].

Due to significant differences in the fit parameters as a function of rapidity and transverse momentum, it is difficult to compare results from experiments with different acceptances directly. This study shows the fit parameters from CERN experiments NA35 and NA44 are consistent within the framework of RQMD.

The decrease of the λ parameter as a function of decreasing p_T is understood in terms of a large radius component, mainly due to long-lived resonance decay. It has been shown previously [15] that kaons are much less affected by long-lived resonance decay and therefore studying kaon correlation functions alleviates this problem.

The p_T dependence of the radius parameters arises from position-momentum correlations in the source. The transverse expansion which causes this correlation is driven in the RQMD model by rescattering. The exclusion of long-lived resonances from the event sample has little effect on the resulting radius parameters and no effect on their trends as a function of p_T.

The comparison of the fit parameters derived from RQMD events to the source space-time distributions indicates that radius parameters give smaller values than the widths of the source distributions. This has been shown to be due to expansion leading to position-momentum

correlations in the source at freeze-out. The relationship between the two transverse radius parameters [Eq. (15)], which should ideally reflect the source lifetime, only holds at very low p_T, where the effect of expansion is minimal. Experiments should look carefully at this p_T region at mid-rapidity for indications of an extended source lifetime, a possible signature of a phase transition from a quark-gluon plasma to normal hadronic matter.

ACKNOWLEDGMENTS

The authors would like to thank J. R. Nix, S. Pratt, W. Willis, and W. Zajc for useful discussions on this topic. We would also like to thank H. Sorge for providing the RQMD code to us. This work was supported by the U.S. Department of Energy under Contracts No. W-31-109-ENG-38 and No. W-7405-ENG-36.

[1] G. Goldhaber, S. Goldhaber, W. Lee, and A. Pais, Phys. Rev. **120**, 300 (1960).
[2] S. Pratt, Phys. Rev. D **33**, 1314 (1986).
[3] G. Bertsch and G. E. Brown, Phys. Rev. C **40**, 1830 (1989).
[4] H. Boggild *et al.*, Phys. Lett. B **302**, 510 (1993).
[5] G. Roland *et al.*, Nucl. Phys. **A566**, 527c (1994).
[6] H. Becker *et al.*, Phys. Rev. Lett. **74**, 3340 (1995).
[7] J. Barrette *et al.*, Phys. Lett. B **333**, 33 (1994).
[8] T. Alber *et al.*, Phys. Rev. Lett. **74**, 1303 (1995).
[9] W. A. Zajc, in *A Pedestrians Guide to Interferometry*, Particle Production in Highly Excited Matter, edited by H. Gutbrod and J. Rafelski, NATO ASI Series, Series B: Physics (Plenum, New York, 1993), Vol. 303, p. 435.
[10] W. A. Zajc, Nucl. Phys. **A525**, 135c (1991).
[11] G. Bertsch, M. Gong, and M. Tohyama, Phys. Rev. C **37**, 1896 (1988).
[12] M. Gyulassy, S. K. Kauffmann, and L. W. Wilson, Phys. Rev. C **20**, 2267 (1979).
[13] S. Chapman, P. Scotto, and U. Heinz, Phys. Rev. Lett. **74**, 4400 (1995).
[14] H. Becker *et al.*, Z. Phys. C **64**, 209 (1994).
[15] J. P. Sullivan, M. Berenguer, B. V. Jacak, S. Pratt, M. Sarabura, J. Simon-Gillo, H. Sorge, and H. van Hecke, Phys. Rev. Lett. **70**, 3000 (1993).
[16] H. Sorge, H. Stöcker, and W. Greiner, Nucl. Phys. **A498**, 567c (1989); H. Sorge *et al.*, Z. Phys. C **47**, 629 (1990).
[17] R. Mattiello, H. Sorge, H. Stöcker, and W. Greiner, Phys. Rev. Lett. **63**, 1459 (1989).
[18] H. Sorge, A. von Keitz, R. Mattiello, H. Stöcker, and W. Greiner, Phys. Lett. B **243**, 7 (1990).
[19] E. V. Shuryak, *The QCD Vacuum, Hadrons, and the Superdense Matter* (World Scientific, Singapore, 1988), p. 341.
[20] S. S. Padula and M. Gyulassy, Nucl. Phys. **B339**, 378 (1990).
[21] N. Xu, *Advances in Nuclear Dynamics*, Proceedings of the 10th Winter Workshop on Nuclear Dynamics, edited by J. Harris *et al.* (World Scientific, Singapore, 1992), p. 86.
[22] S. Chapman, R. J. Nix, and U. Heinz, Phys. Rev. C (submitted).

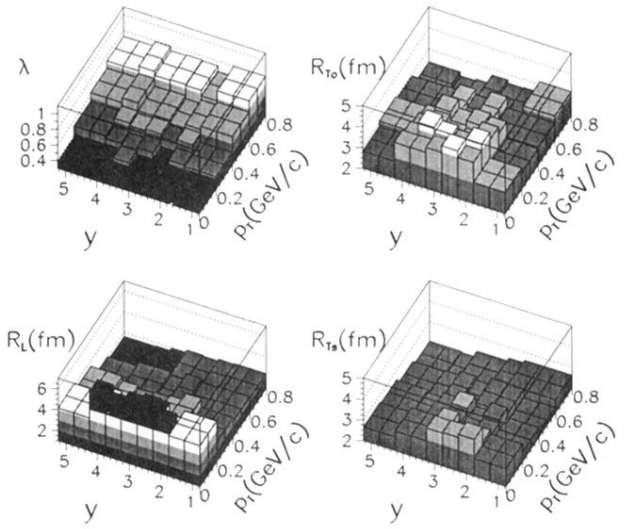

FIG. 2. Fit parameters from pion correlation functions derived from $E/A = 220$ GeV, S+Pb RQMD events as a function of rapidity y, and transverse momentum p_T. Acceptances in rapidity and p_T for the correlation functions are as listed in Table I. (Note that at low and high rapidity and at high p_T the acceptance are more than one bin.)

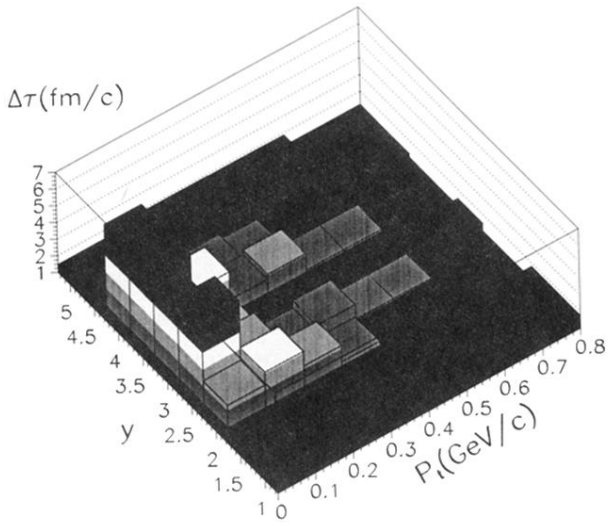

FIG. 3. The width of the emission time distribution τ as calculated from R_{T_0} and R_{T_s} from Table I and Eq. (15). The value of the pair velocity, $\beta_{\pi\pi}$, is determined from the mean p_T in the acceptance.

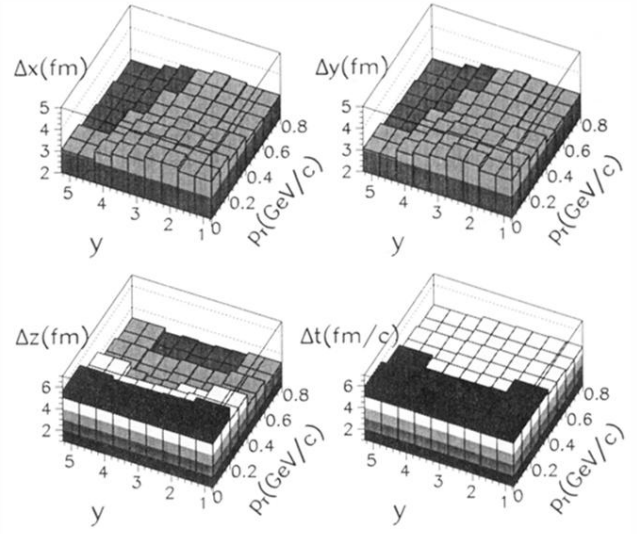

FIG. 4. The widths of the space-time distributions for the same events used to calculate the correlation functions of Fig. 2 (see text for details).

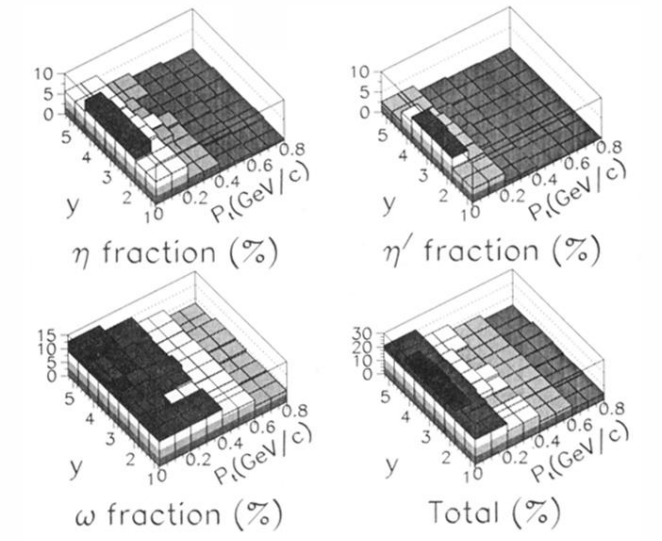

FIG. 7. Relative fraction of pions from resonance decay for three of the most important long-lived resonances. The total fraction of pions from these resonances is also shown.

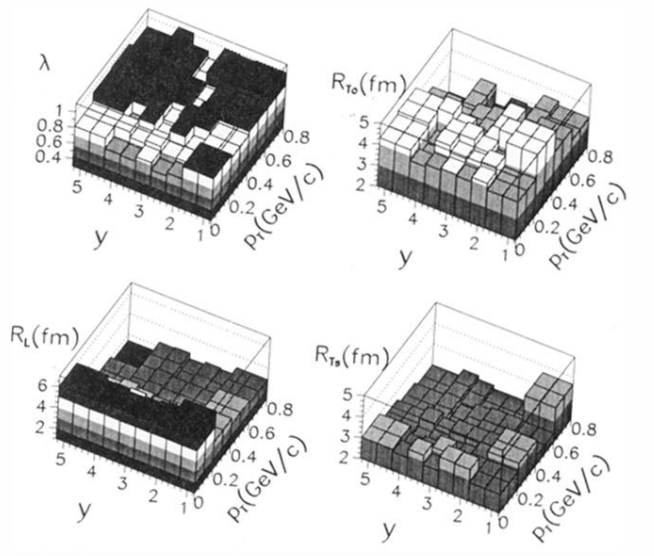

FIG. 8. Fit parameters from correlation functions derived from the same events as Fig. 2, with the resonances of Fig. 7 excluded. The Coulomb part of the wave function was also omitted and no Gamow correction applied.

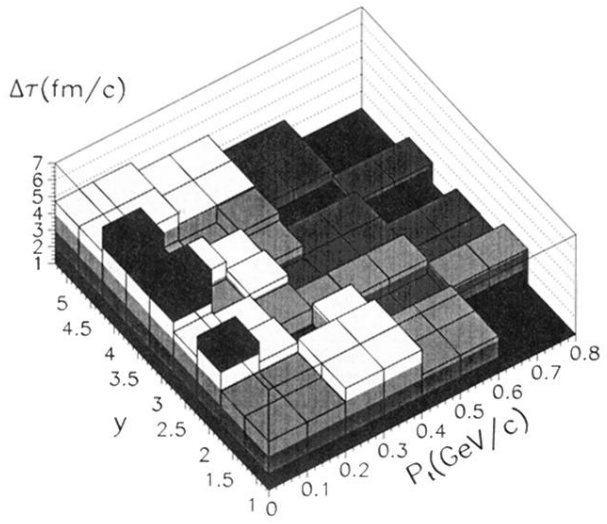

FIG. 9. The width of the emission time distribution τ as calculated from R and R_{T_s} from Fig. 8 and Eq. (15).